View metadata, citation and similar papers at core.ac.uk

brought to you by CORE

provided by Calhoun, Institutional Archive of the Naval Postgraduate School

NAVAL POSTGRADUATE SCHOOL

Monterey, California

THE PROPAGATION OF TIME HARMONIC RAYLEIGH - LAMB WAVES IN A BIMATERIAL PLATE

Clyde Scandrett

Naresh Vasudevan

November 1989

Approved for public release; distribution unlimited
Prepared for: Naval Postgraduate School
Monterey, CA 93943

FedDocs
D 208.14/2
NPS-53-90-001

DUDLEY KNOX LIBRARY
NAVAL POSTGRADUATE SCHOOL
MONTEREY, CALIFORNIA 93943-5002

NAVAL POSTGRADUATE SCHOOL
MONTEREY, CALIFORNIA

Rear Admiral R. W. West, Jr.
Superintendent

Harrison Shull
Provost

This report was prepared in conjunction with research conducted for the Naval Postgraduate School and funded by the Naval Postgraduate School. Reproduction of all or part of this report is authorized.

Prepared by:

REPORT DOCUMENTATION PAGE

NAVAL POSTGRADUATE SCHOOL
MONTEREY, CALIFORNIA 93943-5002

EPORT SECURITY CLASSIFICATION NCLASSIFIED	1b RESTRICTIVE MARKINGS
ECURITY CLASSIFICATION AUTHORITY	3 DISTRIBUTION / AVAILABILITY OF REPORT Approved for public release; distribution unlimited
ECLASSIFICATION / DOWNGRADING SCHEDULE	
REFORMING ORGANIZATION REPORT NUMBER(S) PS-53-90-001	5 MONITORING ORGANIZATION REPORT NUMBER(S) NPS-53-90-001
AME OF PERFORMING ORGANIZATION al Postgraduate School	6b OFFICE SYMBOL (If applicable) 53
7a NAME OF MONITORING ORGANIZATION Naval Postgraduate School	
DDRESS (City, State, and ZIP Code) terey, CA 93943	7b ADDRESS (City, State, and ZIP Code) Monterey, CA 93943
AME OF FUNDING / SPONSORING RGANIZATION al Postgraduate School	8b OFFICE SYMBOL (If applicable) 53
9 PROCUREMENT INSTRUMENT IDENTIFICATION NUMBER O&MN Direct Funding	
DDRESS (City, State, and ZIP Code) terey, CA 93943	10 SOURCE OF FUNDING NUMBERS

PROGRAM ELEMENT NO	PROJECT NO	TASK NO.	WORK UNIT ACCESSION NO

TLE (Include Security Classification)
Propagation of Time Harmonic Rayleigh-Lamb Waves in a Bimaterial Plate

ERSONAL AUTHOR(S) Clyde Scandrett and Naresh Vasudevan

YPE OF REPORT	13b TIME COVERED	14 DATE OF REPORT (Year, Month, Day)	15 PAGE COUNT
nnical Report	FROM 10/88 TO 9/89	7 November 1989	26

UPPLEMENTARY NOTATION

COSATI CODES			18 SUBJECT TERMS (Continue on reverse if necessary and identify by block number)
IELD	GROUP	SUB GROUP	Harmonic, Bimaterial Plate, isotropic, linearly elastic eigenmodes

BSTRACT (Continue on reverse if necessary and identify by block number)

present study involves two semi-infinite homogeneous, isotropic, linearly elastic plates fectly bonded end to end. The plates have dissimilar material properties (e.g. copper and minum). Incident on the interface are both the lowest symmetric and the lowest lsymmetric Rayleigh-Lamb eigenmodes. The resulting transmitted and reflected fields contain tributions from all of the real, imaginary and complex plate modes which are active at the en excitation frequency. A study of the distribution of energy among the various reflected transmitted Rayleigh-Lamb eigenmodes over a range of frequencies is undertaken for a ber of material combinations of the bimaterial plate.

ISTRIBUTION / AVAILABILITY OF ABSTRACT INCLASSIFIED/UNLIMITED ☐ SAME AS RPT ☐ DTIC USERS	21 ABSTRACT SECURITY CLASSIFICATION UNCLASSIFIED
AME OF RESPONSIBLE INDIVIDUAL de Scandrett & Naresh Vasudevan	22b TELEPHONE (Include Area Code) (408) 646-2027
	22c OFFICE SYMBOL 53Sd

ORM 1473, 84 MAR 83 APR edition may be used until exhausted
All other editions are obsolete

SECURITY CLASSIFICATION OF THIS PAGE
UNCLASSIFIED

The Propagation of Time Harmonic Rayleigh-Lamb Waves in a Bimaterial Plate

by

Clyde Scandrett and Naresh Vasudevan [1]
Mathematics Department
Naval Postgraduate School
Monterey, CA 93942

[1] Member, Acoustical Society of America

Abstract

The present study involves two semi-infinite homogeneous, isotropic, linearly elastic plates perfectly bonded end to end. The plates have dissimilar material properties (e.g. copper and aluminum). Incident on the interface are both the lowest symmetric and the lowest antisymmetric Rayleigh-Lamb eigenmodes. The resulting transmitted and reflected fields contain contributions from all of the real, imaginary and complex plate modes which are active at the given excitation frequency. A study of the distribution of energy among the various reflected and transmitted Rayleigh-Lamb eigenmodes over a range of frequencies is undertaken for a number of material combinations of the bimaterial plate.

I. Introduction

Much of the motivation behind the development of theoretical response curves for structures has to do with the nondestructive characterization of their components, and in particular, those undergoing fatigue loading and slow crack growth. Early detection of insipient flaws through studies of the scattering of high frequency elastic waves has received considerable attention in recent years (**Ensminger(1988)**).

The forced response of homogeneous plates to surface and buried sources has been reported in numerous papers (**Ceranoglu et al (1981), Weaver et al (1983), Vasudevan et al (1985)**). Detailed analyses have also been carried out on plane layered systems including plates and half-spaces (**Kennet (1983), Harkrider (1964), Haskell (1953)**). These studies have shown that the dynamic response of a structure is primarily affected by the nature of the source and by the dispersive wave motion induced by the geometry of the structure. Early references regarding infinite and semi-infinite plates can be found in the monograph by **Miklowitz (1978)** and the two volume work of **Auld (1973)**.

Recently, the technique of eigenfunction expansions has been exploited in the papers of **Gregory and Gladwell (1983,1984)**. These authors successfully tackled problems relating to semi-infinite plates by expanding the unknown displacement and stress fields into infinite series of eigenmodes appended with unknown coefficients. The coefficients were found by employing a biorthogonality relationship **(Fraser(1976))** between the eigenmodes.

In this paper, a similar procedure is used to study the elastodynamic response of two dissimilar semi-infinite plates welded along their lateral boundaries. Working in the frequency domain, the spectral response is found by representing the unknown displacements and stress fields in each plate as infinite sums of Rayleigh-Lamb modes. Numerical results are presented for the case of an incident field composed of both the lowest symmetric and the lowest antisymmetric Rayleigh-Lamb modes. The distribution of energy among the modes in the reflected and transmitted fields is numerically studied over a range of excitation frequencies.

II. Formulation and Theory

Shown in figure (1a) are two elastic plates of uniform thickness $2h$ welded at $x = 0$, with P-wave speeds α_1, α_2; S-wave speeds β_1, β_2; densities ρ_1, ρ_2; and shear moduli μ_1, μ_2. The problem addressed is essentially a two dimensional, plane strain scattering problem. A given incident field propagates towards the interface from left to right, which upon striking the interface, generates transmitted and reflected wavefields. The objective of the present analysis is to study the modal contributions to these fields. For an infinite homogeneous plate the only field present should be the incident field. However, when the two plates differ in material properties, waves incident on the interface boundary at $x = 0$ produce reflections which combined with the incident waves yield the total field for $x < 0$. This field must match that of the transmitted field ($x > 0$) along the interface at $x = 0$. In all of the following equations, the time dependence ($e^{-i\omega t}$), has been suppressed.

For a general type of source the incident field can be expanded in the form,

$$\mathbf{u}^{(i)}(x,y) = \sum_{n=1}^{\infty} P_n \mathbf{U}_S^{(n)}(y) e^{ik_n x} + \sum_{n=1}^{\infty} Q_n \mathbf{U}_{AS}^{(n)}(y) e^{iq_n x} \tag{1}$$

where $\mathbf{U}_S^{(n)}(y)e^{ik_n x}$ is the displacement field of the n^{th} symmetric Rayleigh-Lamb mode of the plate, and the wave number k_n is a root of the symmetric Rayleigh-Lamb frequency equation. The boldface lettering of U signifies that it is a two-vector. In a similar fashion, the subscript AS refers to the antisymmetric modes of the plate and the wave number q_n is a root of the antisymmetric Rayleigh-Lamb frequency equation. The expressions for the mode shapes as well as that for the frequency equations are stated in Appendix A. It is presumed that the homogeneous problem can be solved and thus the coefficients P_n and Q_n are known. The first series in the expression for $\mathbf{u}^{(i)}$ of equation (1) will excite symmetric modes while the second series will excite only antisymmetric modes. For the purposes of the present study, all coefficients of the incident field are zero except the first term in each series which is identically one. However, the mathematical formulation presented below is applicable for an arbitrary source field.

For $x < 0$ the reflected field can be expressed as:

$$\mathbf{u}^{(r)}(x,y) = \sum_{n=1}^{\infty} R_n \bar{\mathbf{U}}_S^{(n)}(y) e^{-ik_n x} + \sum_{n=1}^{\infty} S_n \bar{\mathbf{U}}_{AS}^{(n)}(y) e^{-iq_n x}, \tag{2}$$

which represents leftward travelling waves (the overbar indicates complex conjugation). The coefficients R_n and S_n are to be determined from the continuity conditions valid at the interface.

The transmitted field for the region $x > 0$, takes the form :

$$\mathbf{u}^{(t)}(x,y) = \sum_{n=1}^{\infty} \hat{R}_n \hat{\mathbf{U}}_S^{(n)}(y) e^{i\hat{k}_n x} + \sum_{n=1}^{\infty} \hat{S}_n \hat{\mathbf{U}}_{AS}^{(n)}(y) e^{i\hat{q}_n x}, \tag{3}$$

where the 'hat' symbol is used to indicate that there is a different set of elastic constants to be considered for $x > 0$.

All of the mode shapes in equations (2-3) satisfy traction free boundary conditions on the free surfaces of the plates ($y = \pm h$). For a perfectly welded interface, the total displacement and stress fields in the two plates must be continuous across $x = 0$.

The symmetric and antisymmetric portions of the fields are split with continuity being imposed on each separately. In what follows, only the determination of the coefficients for the symmetric case is given. A similar procedure can be performed to determine coefficients for the antisymmetric modes. Enforcing stress and displacement continuity across the boundary at $x = 0$ yields:

(4a) $$\sum_{n=1}^{\infty} P_n U_x^{(n)} + \sum_{n=1}^{\infty} R_n \bar{U}_x^{(n)} = \sum_{n=1}^{\infty} \hat{R}_n \hat{U}_x^{(n)}$$

(4b) $$\sum_{n=1}^{\infty} P_n U_y^{(n)} + \sum_{n=1}^{\infty} R_n \bar{U}_y^{(n)} = \sum_{n=1}^{\infty} \hat{R}_n \hat{U}_y^{(n)}$$

(4c) $$\mu_1 \sum_{n=1}^{\infty} P_n S_{xx}^{(n)} + \mu_1 \sum_{n=1}^{\infty} R_n \bar{S}_{xx}^{(n)} = \mu_2 \sum_{n=1}^{\infty} \hat{R}_n \hat{S}_{xx}^{(n)}$$

(4d) $$\mu_1 \sum_{n=1}^{\infty} P_n S_{xy}^{(n)} + \mu_1 \sum_{n=1}^{\infty} R_n \bar{S}_{xy}^{(n)} = \mu_2 \sum_{n=1}^{\infty} \hat{R}_n \hat{S}_{xy}^{(n)}.$$

In equations (4a-d) U_x and U_y are the x and y components of the displacement vector $\tilde{\mathbf{U}}_S$ while S_{xx} and S_{xy} are the corresponding components of the symmetric stress vector $\tilde{\mathbf{S}}_S$ (given in the appendix). The complex conjugates of the displacement and stress components satisfy the following relations:

(5a) $$\bar{U}_x^{(n)} = -U_x^{(n)}; \qquad \bar{U}_y^{(n)} = U_y^{(n)}$$

(5b) $$\bar{S}_{xx}^{(n)} = S_{xx}^{(n)}; \qquad \bar{S}_{xy}^{(n)} = -S_{xy}^{(n)}$$

Using the above relations, equation (4) is rewritten as:

(6a) $$\sum_{n=1}^{\infty} (P_n - R_n) U_x^{(n)} = \sum_{n=1}^{\infty} \hat{R}_n \hat{U}_x^{(n)}$$

(6b) $$\sum_{n=1}^{\infty}(P_n + R_n)U_y^{(n)} = \sum_{n=1}^{\infty}\hat{R}_n\hat{U}_y^{(n)}$$

(6c) $$\mu_1\sum_{n=1}^{\infty}(P_n + R_n)S_{xx}^{(n)} = \mu_2\sum_{n=1}^{\infty}\hat{R}_n\hat{S}_{xx}^{(n)}$$

(6d) $$\mu_1\sum_{n=1}^{\infty}(P_n - R_n)S_{xy}^{(n)} = \mu_2\sum_{n=1}^{\infty}\hat{R}_n\hat{S}_{xy}^{(n)}.$$

The infinite systems of equations (6a-d) must be satisfied for $-h < y < h$. A procedure to eliminate the thickness variable (y) from equations (6a-d) employs a biorthogonality relation valid for elastic plates. This relation is stated in Appendix A as equation (9A). Equation (6a) is multiplied by $\mu_1 S_{xx}^{(m)}$ (where the superscript (m) refers to the m^{th} mode) and added to equation (6d) multiplied by $-U_y^{(m)}$. The resulting equation is then integrated with respect to y from $-h$ to $+h$. In similar fashion, equation (6b) is multiplied by $\mu_2\hat{S}_{xy}^{(m)}$, equation(6c) is multiplied by $-\hat{U}_x^{(m)}$ and the two are added and integrated over the plate thickness. The biorthogonality relation reduces the resulting pair of equations to the form :

(7) $$(R_m - P_m)J_m = \sum_{n=1}^{\infty}\hat{R}_n K_{mn}$$

(8) $$\sum_{n=1}^{\infty}(P_n + R_n)L_{mn} = \hat{R}_m Q_m.$$

In the above,

(9a) $$K_{mn} = \int_{-h}^{h}(-\mu_2 U_y^{(m)}\hat{S}_{xy}^{(n)} + \mu_1\hat{U}_x^{(n)}S_{xx}^{(m)})dy$$

(9b) $$L_{mn} = -K_{nm}.$$

In order to cast equations (7) and (8) into tensor form diagonal matrices J_{ij} and Q_{ij} are introduced and defined in equations (12a,b). The quantities J_m and Q_m in equations (7,8) are the nonzero diagonal entries defined in equation(12). Notice that whereas J_m and Q_m involve only the properties of the left and right hand side of the plates respectively, the coefficient K_{mn} is a coupling term that combines the properties of both materials.

Equations (7) and (8) constitute an infinite system of equations for the infinite number of unknowns R_m and $\hat{R}_m$. To proceed with the numerical calculations, the infinite series is truncated after N terms. Ideally, the value of N should be chosen in such a way that the magnitude of the truncated terms is smaller than a specified tolerance. In the present case a practical procedure was adopted. If an increase in the value of N was found to to have an indiscernible effect on the output, that value of N was chosen as final. In physical terms truncation implies that the influence of higher modes is relatively small. Rewriting the truncated equations (7-8) in tensor notation yields:

$$\mathbf{J}_{ij}\mathbf{R}_j - \mathbf{K}_{ij}\hat{\mathbf{R}}_j = \mathbf{J}_{ij}\mathbf{P}_j \tag{10}$$

$$\mathbf{L}_{ij}\mathbf{R}_j - \mathbf{Q}_{ij}\hat{\mathbf{R}}_j = -\mathbf{L}_{ij}\mathbf{P}_j \tag{11}$$

where $\mathbf{J}_{ij}$ and $\mathbf{Q}_{ij}$ are NxN diagonal matrices involving material properties from the left and right plates respectively;

$$J_{ij} = \begin{cases} 0 & i \neq j \\ \mu_1 \displaystyle\int_{-h}^{h} (-U_y^{(j)} S_{xy}^{(j)} + U_x^{(j)} S_{xx}^{(j)}) dy & i = j \end{cases} \tag{12a}$$

$$Q_{ij} = \begin{cases} 0 & i \neq j \\ \mu_2 \displaystyle\int_{-h}^{h} (-\hat{U}_y^{(j)} \hat{S}_{xy}^{(j)} + \hat{U}_x^{(j)} \hat{S}_{xx}^{(j)}) dy & i = j \end{cases}; \tag{12b}$$

and $\mathbf{K}_{ij}$ and $\mathbf{L}_{ij}$ are NxN full complex matrices given in equations (9a-b). The quantities R and $\hat{R}$ are N dimensional vectors containing the unknown reflection and transmission coefficients respectively. The right hand side of equations (10,11) involve the vector P which contains the known incident field coefficients. Letting $\mathbf{Z} = \mathbf{J}_{ij}\mathbf{P}_j$ and $\hat{\mathbf{Z}} = -\mathbf{L}_{ij}\mathbf{P}_j$, equations (10) and (11) can be written as a 2Nx2N matrix equation as follows:

$$\begin{bmatrix} \mathbf{J} & \mathbf{L}^T \\ \mathbf{L} & -\mathbf{Q} \end{bmatrix} \begin{bmatrix} \mathbf{R} \\ \hat{\mathbf{R}} \end{bmatrix} = \begin{bmatrix} \mathbf{Z} \\ \hat{\mathbf{Z}} \end{bmatrix}. \tag{13}$$

The task of determining the symmetric reflection and transmission coefficients is reduced to solving equation (13), or, as is done in the present work, solving equations (10) and (11). A similar process yields the antisymmetric coefficients.

Having obtained the coefficients, an analysis of the stress and displacement fields in either plate can be undertaken. Of particular interest is the fraction of the incident energy flux carried away by each real reflected and transmitted mode. Following **Gregory and**

Gladwell(1983), the fraction of energy flux carried by each real eigenmode at a particular frequency is given by :

(14a) $$E_j = |Im(J_j)/Im(J_1)|||R_j||^2,$$

for reflected, and

(14b) $$\hat{E}_j = |Im(Q_j)/Im(J_1)|||\hat{R}_j||^2$$

for transmitted modes respectively. "Edge"modes corresponding to Rayleigh-Lamb eigenvalues with nonzero imaginary components transmit no energy and therefore their energy fractions are set to zero. It must be kept in mind however, that while the imaginary and complex modes do not transport energy they affect the magnitude of the coefficients R and $\hat{R}$ and therefore the energy partitioning.

III. Numerical Procedure

In order to set up the matrix equations (10-11) of the previous section it is necessary to calculate the roots of the Rayleigh-Lamb frequency equation, from which the mode shapes can be determined and ultimately the matrix entries. In the present work a method which closely parallels that of **Gregory and Gladwell (1983)** is adopted which tracks a prescribed number of roots over a range of frequencies. These root finding routines (for both anti-symmetric and symmetric modes) are called intermittently by a main program which solves the matrix equations (10-11) and calculates the fractional amount of energy transported by each real mode using equations (14a,b).

Initially the roots of the following two equations:

$$sinh(2k_n h) \pm 2k_n h = 0 \tag{15}$$

are found for a prescribed number of modes. The equation with the "plus"sign is associated with the symmetric roots of the Rayleigh- Lamb frequency equation as the frequency approaches zero, while the equation with the negative sign corresponds to the anti-symmetric Rayleigh-Lamb equation.

As the frequency is increased, updated values of k_n are found by employing a Newton iteration scheme when k_n is complex and a bisection algorithm if k_n is either purely imaginary or purely real. When the real or imaginary parts of k_n change sign, the value of k_n becomes purely real or purely imaginary. In such instances, a left hand turn rule has been adopted to ensure that modes propagating with the correct group velocity have been selected.

Figures (1b, 1c) illustrate the paths taken in tracking a few of the lowest symmetric and anti-symmetric modes of a plate of glass which has a Poissons' ratio of nearly .25. Each of the curves have been labelled with a number (signifying the mode) and a letter (identifying that portion of the curve as complex, real, or imaginary).The base axis on the right is the real axis, while that on the left is the imaginary axis. The vertical axis is frequency in megahertz. While the vertical axis is labelled up to 1 megahertz, the curves do not have data points beyond .738 megahertz for the antisymmetric roots, and .696 megahertz for the symmetric roots. In addition, curves extending beyond the boundaries of the graph have been truncated.

Rather than give a detailed explanation and description for each curve, attention will be focused on the third symmetric root since it displays as complicated a route as can be seen in any of the remaining curves. The third symmetric root (k_3) is initially complex. At .275 megahertz k_3 intersects the real plane and becomes purely real. At this point, the third mode has a negative phase velocity and a positive group velocity. At .291 megahertz, which agrees with the theoretical value of the first cutoff, k_3 intersects the imaginary plane and becomes purely imaginary. It makes a loop in the imaginary plane, intersecting the real plane at .336 and becomes purely real (this value corresponds to the second theoretical cutoff).

Numerical Results and Discussion

In each numerical simulation left to right travelling symmetric(S) and antisymmetric(AS) fundamental modes with unit energy flux are incident upon the bimaterial plate interface. The unknown amplitude coefficients in equations (2-3) are found by solving the matrix equations (10-11), from which the energy fractions can be computed using equations (14a,b).

The values of N are fixed at 21 for symmetric and 20 for antisymmetric modes in each of the numerical experiments reported below. Greater values of N than those chosen were found to produce indiscernible changes in the amounts of energy fractions as displayed in the graphs to follow. The choices for N were determined from a sensitivity analysis of the output to varying N. Results of this analysis are presented in tables I and II, where the two materials are aluminum and steel (corresponding to the first numerical experiment described in detail below). The tables include the energy partitions of the antisymmetric reflected and transmitted modes at two frequencies (results for the symmetric case show equivalent convergence). The higher frequency corresponds to a Rayleigh wavelength of about 1/3 of the plate thickness and the lower frequency about twice that. Tabulated are the energy fractions for the first four modes found by taking N equal to 2, 6, 10 and 20 in the calculations. Notice from the tables that there is not a substantial difference between the convergence at 10 and 20 modes with between two to four significant digits remaining unchanged.

It should be noted that in the following table as well as for all of the results presented, the sum of the energy fractions equal 1 to at least five places (for symmetric as well as antisymmetric cases) for each value of N and at every frequency point for which the energy was evaluated. This provides a small measure of confidence in the numerical calculations as well as indicating that energy conservation cannot be used in determining convergence of the eigenfunction expansion series.

The first pair of materials considered are Aluminum and Steel with the incident wave originating in Aluminum. In all of the examples considered the plate thickness is taken to be 1 cm. The elastic properties of Aluminum used are: a P-wave speed of 6.15 Km/sec, an S-wave speed of 3.10 Km/sec, and a density of 2.5 gm/cc. Aluminum is soft in comparison with Steel for which the P-wave speed, S-wave speed, and density are taken to be: 5.76 Km/sec, 3.16 Km/sec, and 7.8 gm/cc. In figures 2 and 3 are shown the fraction of incident energy carried away by each mode for the symmetric and antisymmetric excitations respectively. The upper plot in each of the following figures represents the reflected field and the lower plot the transmitted field. The upper limit of frequency chosen is high enough to include the effect of up to 4 real modes in either plate material.

A noteworthy feature of the behaviour of the lowest S mode in figure 2 is the sharp maximum in the reflected field in Aluminum just beyond the point denoted by R_1 and the corresponding minimum in transmission just beyond T_1. This sharp maximum in reflection also marks the beginning of the negative phase velocity branch of the third S mode for steel shown by the dashed curve. The next prominent feature for the lowest mode occurs near R_2, T_2 which marks the beginning of the cutoff of the third S mode for Aluminum. The peak in the dashed curve near R_2 corresponds to the local minimum near T_2 in the fundamental mode in transmission. Shortly thereafter the third real mode

for Steel becomes activated causing the transmission curve for the first S mode to rise again. The next fluctuation in the curves occurs in the region of R_3, T_3. Again, observe that the fourth S mode for Aluminum is activated before its counterpart in Steel. Hence there is first an increase in the reflection curve for all four modes in Aluminum. Soon thereafter the fourth S mode in Steel becomes active causing a rise in transmission with a corresponding drop in reflection. This feature is characteristic of all the curves where a maxima in the reflected energy corresponds to a minima in the transmitted curve or vice versa since the total energy must add up to the incident flux. A general feature of figure 2 is that one sees a blip on the curves for either material at the cutoffs of the other material. This indicates that as a new energy bearing real mode becomes activated in one of the materials there is seen a fluctuation in the energy curve of the other material. This is because of a redistribution of energy among the real modes. Similar features are observed in the subsequent plots.

In figure 3 is shown the results for the antisymmetric case. Once again the cutoff for the second AS mode in Aluminum occurs before that in Steel. Thus there is first a rise in reflected energy followed by a drop as the second cutoff for Steel becomes activated. This phenomenon is somewhat easier to observe in figure 3 than in figure 2 because the negative phase velocity branch for the AS case occurs in the fourth mode. However, for the AS case this negative phase velocity region is present only for a very small range of frequencies as opposed to the third S mode where it is far more conspicuous. The points R_2, T_2 denote the activation of the third mode and R_3, T_3 the activation of the fifth mode. Clearly visible are the windows in the frequency domain where reflection and transmission are approximately uniform followed by steep drops in the neighbourhood of the cutoffs. It appears from these curves that the transmission of energy is done primarily by lowest flexural mode. The higher order AS modes which incorporate most of the shearing deformation is poorly transmitted. A similar feature is observed in the AS case for other combinations of materials.

In figures 4 and 5 are shown the symmetric responses for Aluminum to Copper and Copper to Aluminum respectively. The properties for Copper are a P-wave speed of 4.17 Km/sec, an S-wave speed of 2.15 Km/sec and a density of 9.8 gm/cc. Copper is a denser but softer material than Aluminum.

An interesting feature of these curves is that the transmission curve for the lowest mode is exactly identical whether the transmission is from Copper to Aluminum or vice versa. Figures 6 and 7 show that the same is true for the lowest AS mode as well. In Appendix B we provide an outline of the proof of this 'reciprocity' for any pair of elastic materials. It must be kept in mind that the input excitation consists of the lowest mode and hence the 'reciprocity' is observed only for the lowest transmitted mode.

Since the cutoffs for Copper and Aluminum are well separated, one can observe the phenomena discussed earlier in a somewhat clearer manner. What is particularly remarkable in figure 5 is the large reflection (about 60 percent) in the third S mode (dashed curve) for Aluminum. In figure 4, however, the transmitted energy is largely in the first and *second* symmetric modes of copper. The blips observed on either the reflection or transmission curve are usually stronger at the thickness shear cutoffs as opposed to the thickness stretch cutoffs. This is true in transient loading problems as well, where the

singularities at the thickness shear cutoffs dominate over their dilatational counterparts. In this case, there is a spectral window ranging from about 0.2 to 0.3 Mhz in Copper where transmission in the second S mode is quite strong. The blips at $R_4, T_4, R_3, T_3, R_5, T_5$ occur at the cutoffs of either material. These represent a sudden surge of energy followed by a drop or vice versa once again due to the repartitioning of energy.

In figures 6 and 7 is shown the response to an antisymmetric excitation. As discussed earlier there is little transmission in the higher modes. In figure 7 the dotted and dashed curves display a strong reflectivity. The same is true for figure 6 where the cutoffs (in Aluminum) occur at higher frequencies than those in Copper.

For the problem of transmission of energy across an infinite boundary, 'mechanical impedance' (the product of density and wave speed) is sometimes used as a measure of mismatch between bonded materials. Roughly speaking, this quantity is a qualitative measure of one material's ability to let energy enter or exit into a second material to which it is bonded.

In figures 8 and 9 are shown the results for Aluminum-Glass. These two materials are remarkably well matched in terms of their mechanical impedances. For Glass the wave speeds chosen are: a P-wave speed of 5.80 Km/sec and an S-wave speed of 3.35 Km/sec, while the density is taken to be 2.5 gm/cc. Near perfect transmission can be observed in figure 8 except near the negative phase velocity region of the third S mode for Glass. Almost all the transmitted energy is carried by the fundamental mode for both the symmetric and antisymmetric excitations. The reflection is a thousand times smaller than transmission with the peak occuring in the negative phase region of the third S mode in figure 8. For the antisymmetric case, the transmission is still better in the fundamental mode. The higher modes for both the S and AS cases transmit negligibly tiny fractions of energy.

One of the basic features observed in the foregoing discussion is the interplay between the modes in their energy carrying capabilities. As real modes become activated in the two materials there are corresponding increments or drops in the energy levels in reflection with exactly the opposite being true for transmission. One can view the activation of a new mode as an enhancement in the energy transport capabilities of a given plate material. A second feature of the results presented is the appearance of windows in the frequency domain where a nearly uniform behaviour in energy transmission in certain modes can be seen. More work needs to be done to clarify all of the observed features in the plots presented here. The goal for future work is to obtain solutions to the transient loading problem in bimaterial plates which are of particular relevance to NDE. The technique described in this paper can be easily extended to the case of multiple sandwich sections which may be of interest in waveguide analysis. Work along these lines is currrently in progress.

Tables I and II

Antisymm-Reflected Field				
2 Modes				
Mhz	Mode 1	Mode 2	Mode 3	Mode 4
0.767	0.0794	0.0326	0.0000	0.0000
0.393	0.1060	0.0017	0.0000	0.0000
6 Modes				
0.767	0.3120	0.0003	0.0559	0.1220
0.393	0.1510	0.0058	0.0000	0.0000
10 Modes				
0.767	0.1900	0.0181	0.0369	0.0438
0.393	0.1510	0.0057	0.0000	0.0000
20 Modes				
0.767	0.1920	0.0179	0.0369	0.0454
0.393	0.1510	0.0057	0.0000	0.0000

Antisymm-Transmitted Field				
2 Modes				
Mhz	Mode 1	Mode 2	Mode 3	Mode 4
0.767	0.8870	0.0010	0.0000	0.0000
0.393	0.8870	0.0051	0.0000	0.0000
6 Modes				
0.767	0.3570	0.0364	0.0102	0.1060
0.393	0.8360	0.0071	0.0000	0.0000
10 Modes				
0.767	0.6550	0.0120	0.0039	0.0405
0.393	0.8360	0.0072	0.0000	0.0000
20 Modes				
0.767	0.6490	0.0123	0.0038	0.0418
0.393	0.8360	0.0072	0.0000	0.0000

Appendix A

For a uniform, isotropic plate there exist both symmetric and antisymmetric Rayleigh-Lamb modes which independently satisfy traction free boundary conditions on each surface of the plate ($y = \pm h$). The displacement can be written in vector form as follows:

$$\tilde{\mathbf{u}}^{(n)} = \tilde{\mathbf{U}}^{(n)}(y) e^{ik_n x} e^{-i\omega t} \tag{1A}$$

where the $\tilde{\mathbf{U}}^{(n)}(y)$ are either the symmetric or antisymmetric modes. For example, the symmetric modes are given by,

$$\tilde{\mathbf{U}}^{(n)}(y) = \begin{pmatrix} ik_n ch(\gamma_n y) + \delta_n B_n ch(\delta_n y) \\ \gamma_n sh(\gamma_n y) - ik_n B_n sh(\delta_n y) \end{pmatrix} \tag{2A}$$

The symbols sh and ch refer to the hyberbolic sine and cosine respectively. The quantity k_n which is related to the horizontal component of the wavenumber satisfies a transcendental equation called the Rayleigh-Lamb frequency equation which for symmetric modes can be written,

$$(2k_n^2 - K^2)^2 ch(\gamma_n) sh(\delta_n) - 4k_n^2 \gamma_n \delta_n sh(\gamma_n) ch(\delta_n) = 0 \tag{3A}$$

where

$$\gamma_n = (k_n^2 - k^2)^{1/2} \tag{4A}$$

$$\delta_n = (k_n^2 - K^2)^{1/2} \tag{5A}$$

$$B_n = (2k_n^2 - K^2) ch(\gamma_n) / 2ik_n \delta_n ch(\delta_n). \tag{6A}$$

In the above, k and K are the compression and shear wave numbers respectively. The corresponding stress vector for the n^{th} eigenmode is:

$$\begin{pmatrix} \sigma_{xx}^{(n)} \\ \sigma_{xy}^{(n)} \end{pmatrix} = \mu \tilde{\mathbf{S}}^{(n)}(y) e^{ik_n x} e^{-i\omega t} \tag{7A}$$

where again the $\tilde{\mathbf{S}}^{(n)}$ can be either the stress resulting from the symmetric or antisymmetric displacements. For the symmetric case it is given by:

$$\tilde{\mathbf{S}}^{(n)}(y) = \begin{pmatrix} -(2\gamma_n^2 + K^2) ch(\gamma_n y) + 2ik_n B_n \delta_n ch(\delta_n y) \\ 2ik_n \gamma_n sh(\gamma_n y) + (2k_n^2 - K^2) B_n sh(\delta_n y) \end{pmatrix} \tag{8A}$$

The bi-orthogonality condition for the in-plane problem can now be simply stated as

$$\mu \int_{-h}^{+h} (S_{xy}^{(m)} U_y^{(n)} - U_x^{(m)} S_{xx}^{(n)}) dy = \begin{Bmatrix} 0 & m \neq n \\ J_m & m = n \end{Bmatrix} \tag{9A}$$

Here the subscripted forms of $\tilde{\mathbf{S}}$ and $\tilde{\mathbf{U}}$ represent components of each vector. Notice that the biorthogonality relation involves an integration over the thickness of the plate.

Appendix B

Following is a short argument proving the reciprocity between transmitted fundamental modes of a bimaterial plate noted in the results section of the paper.

In the absence of body forces, the reciprocity theorem (**Achenbach et al (1982)**) between two elastic states (A and B) can be written:

(B1) $$\int_S (u_i^B \tau_{ij}^A - u_i^A \tau_{ij}^B) n_j dA = 0.$$

For the 2D plane strain bimaterial plate problem with plate thickness $2h$, the above integral becomes:

(B2) $$\int_{-h}^{h} (u_i^B \tau_{ij}^A - u_i^A \tau_{ij}^B)_{x=l} dy = \int_{-h}^{h} (u_i^B \tau_{ij}^A - u_i^A \tau_{ij}^B)_{x=-l} dy,$$

where the interface between the two plates is at $x = 0$.

For elastic states A and B consider transmitted and reflected fields (expressed in terms of Rayleigh-Lamb eigenmodes of the appropriate plate) resulting from incident displacements

(B3) $$\mathbf{u}_A^I = \mathbf{U}^{(1)}(y) e^{ik_1 x} / J_1$$

(B4) $$\mathbf{u}_B^I = \bar{\tilde{\mathbf{U}}}^{(1)}(y) e^{iq_1 x} / Q_1$$

where J_1 and Q_1 are given in equations (12a-b). By substitution of the above incident and resulting reflected and transmitted fields into equation (B2) one finds that the coefficients of the leading terms in the transmitted fields of each elastic state are equal.

It should be noted that if the incident field involved additional modes the reciprocity relationship would involve a combination of the corresponding transmitted modes.

References

Achenbach, J. D., Gautesen, A. K., McMaken, H. 1982.**Ray Methods for Waves in Elastic Solids**. Boston: Pitman.

Auld, B. 1973. **Acoustic Fields and Waves in Solids**. New York: Wiley-Interscience.

Ceranoglu, A. N. and Pao, Y. H. 1981. Propagation of elastic pulses and acoustic emission in a plate. Parts I, II, and III. **ASME J. Appl. Mech. 48** :125-147.

Ensminger, D. 1988. **Ultrasonics, Fundamentals, Technology, Applications.** New York: Marcel Dekker, Inc.

Fraser, W. B. 1976. Orthogonality relation for the Rayleigh- Lamb modes of vibration of a plate. **J. Acoust. Soc. Am. 59**: 215-216.

Gregory, R. D. and Gladwell, I. 1983. The reflection of a symmetric Rayleigh-Lamb wave at a fixed or free edge of a plate. **J. Elasticity 13**: 185-206.

Gregory, R. D. and Gladwell, I. 1984. The generation of waves in a semi-infinite plate by a smooth oscillating piston. **ASME J. Appl. Mech. 51**: 787-791.

Harkrider, D. G. 1964. Surface waves in multilayered elastic media. **B.S.S.A. 54**: 627-679.

Haskell, N. A. 1953. The dispersion of surface waves in multilayered media. **B.S.S.A. 43**: 17-34.

Kennet, B. L. N. 1983. **Seismic Wave Propagation in Stratified Media**. Cambridge, Mass.: Cambridge University Press.

Miklowitz, J. 1978. **The Theory of Elastic Waves and Waveguides**. New York: North-Holland.

Vasudevan, N. and Mal, A. K. 1985. Response of an elastic plate to localized transient sources. **ASME J. Appl. Mech. 52**: 1-7.

Weaver, R. L. and Pao, Y. H. 1983. Axisymmetric elastic waves excited by a point source in a plate. **ASME J. Appl. Mech 49**: 821-836.

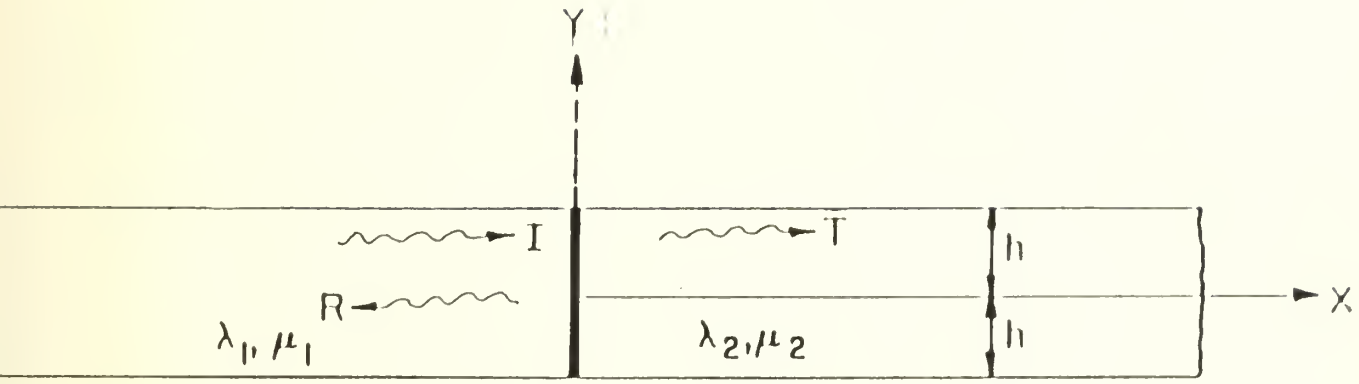

T: Transmitted
R: Reflected
I: Incident

Two semi-infinite plates welded together at $x = 0$

Fig. 1 (a)

symmetric roots: glass

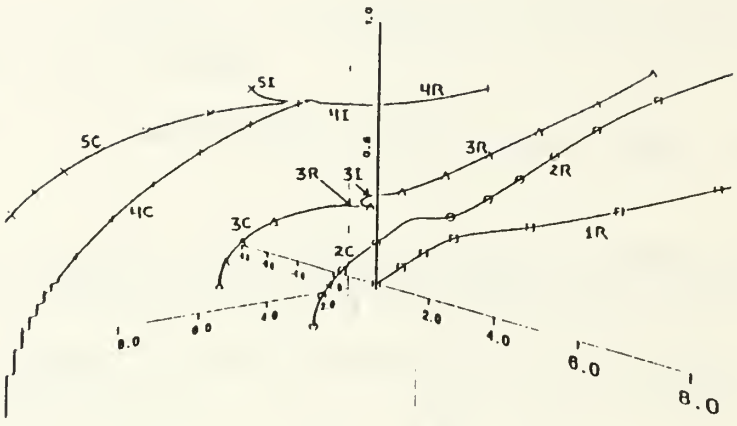

LEGEND
□ = fundamental mode
○ = second mode
△ = third mode
◇ = fourth mode
× = fifth mode

Fig. 1(b)

anti-symmetric roots: glass

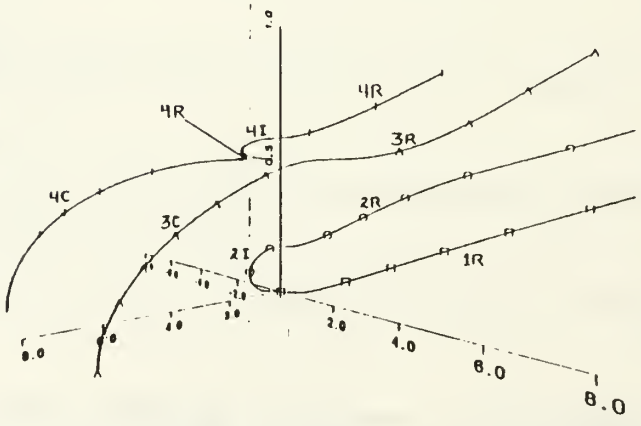

LEGEND
□ = first mode
○ = second mode
△ = third mode
◇ = fourth mode

Fig. 1(c)

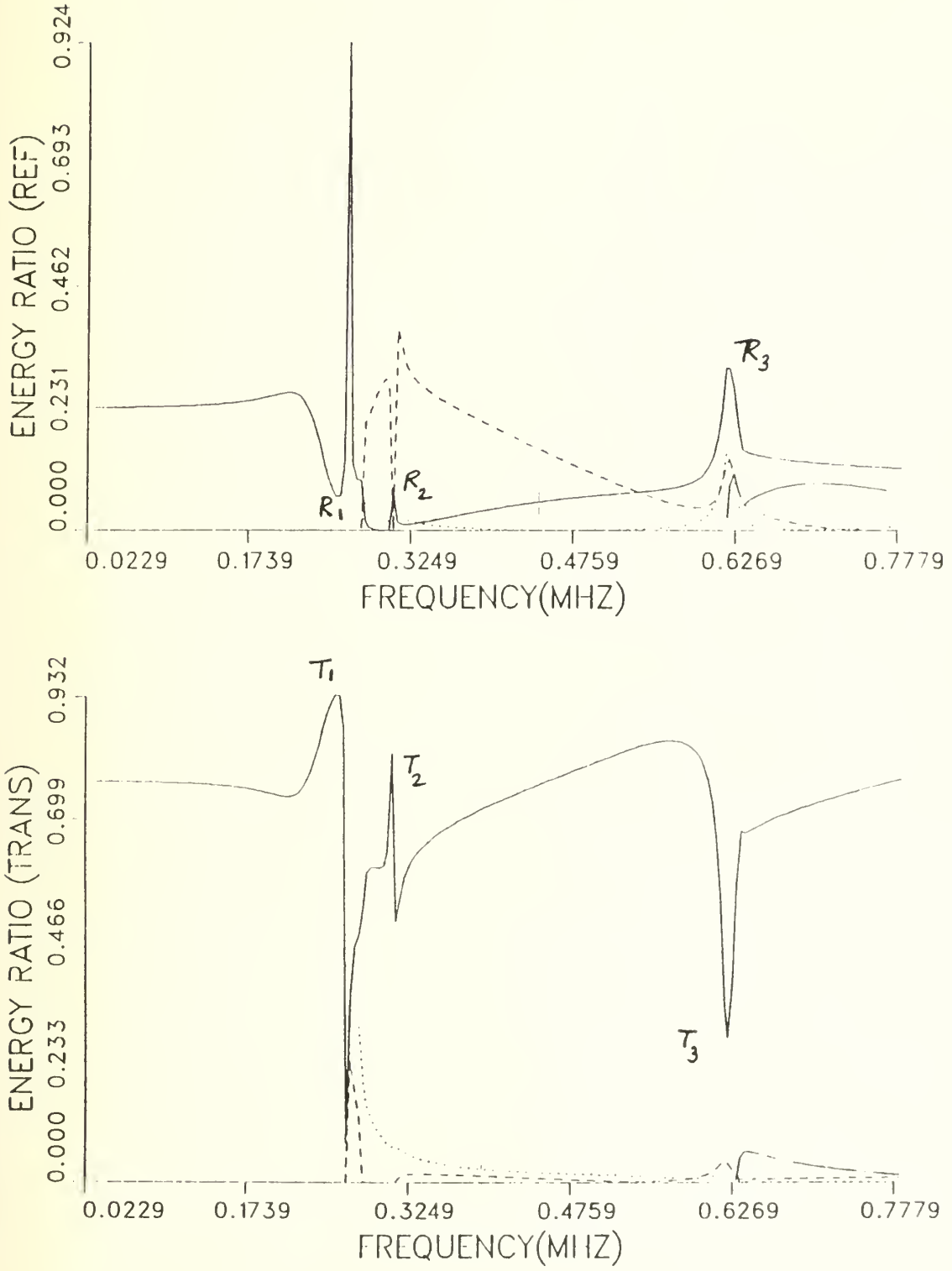
ALUM-STEEL; SYMMETRIC
ENERGY RATIO (REF)
0.000
0.231
0.462
0.693
0.924
R1
R2
R3
0.0229
0.1739
0.3249
0.4759
0.6269
0.7779
FREQUENCY(MHZ)
ENERGY RATIO (TRANS)
0.000
0.233
0.466
0.699
0.932
T1
T2
T3
0.0229
0.1739
0.3249
0.4759
0.6269
0.7779
FREQUENCY(MHZ)
Mode 1
Mode 2
Mode 3
Mode 4

Fig. 2

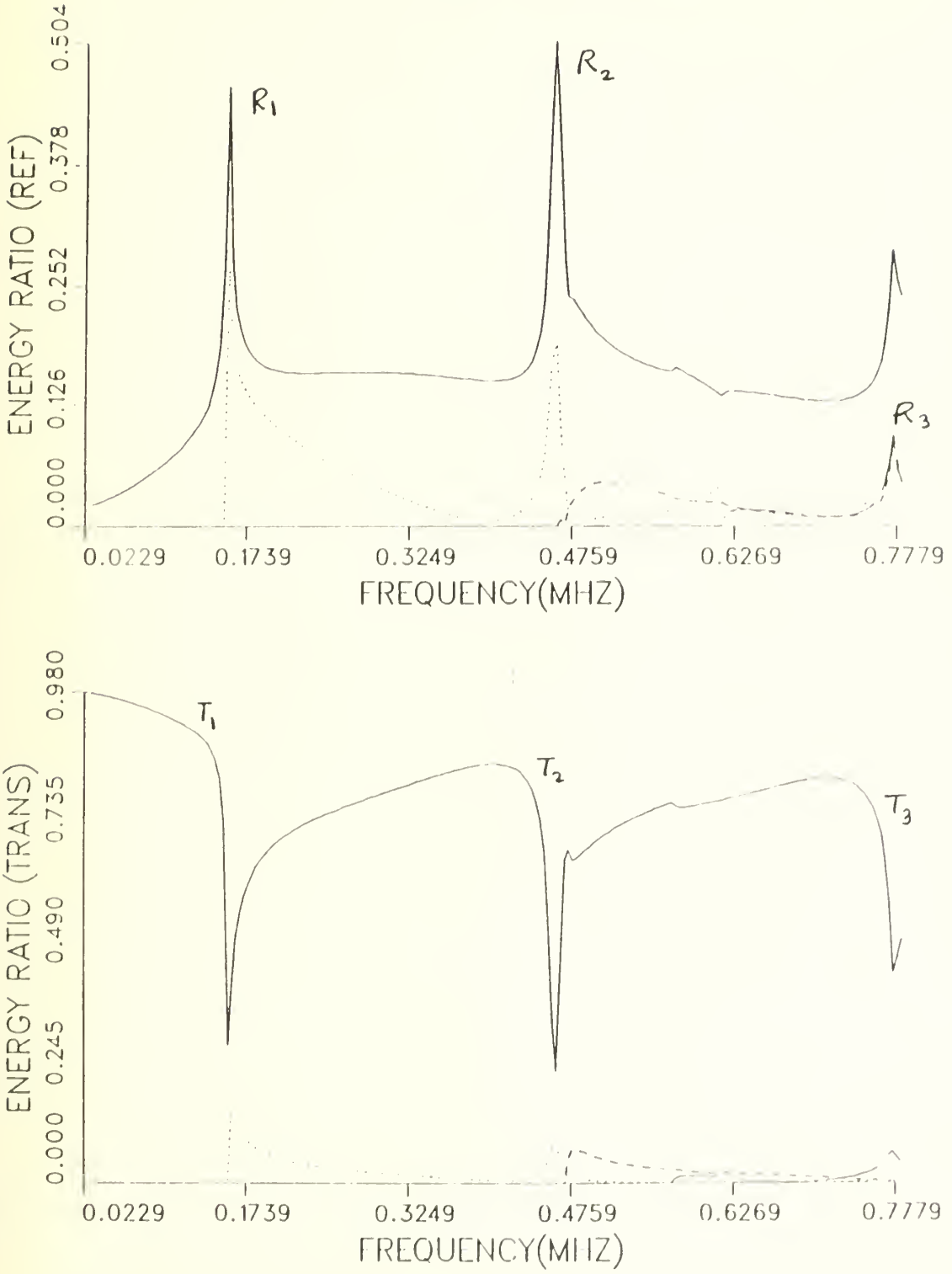

—— Mode 1 ..... Mode 2 - - - - Mode 3 —·—·— Mode 4

Fig. 3

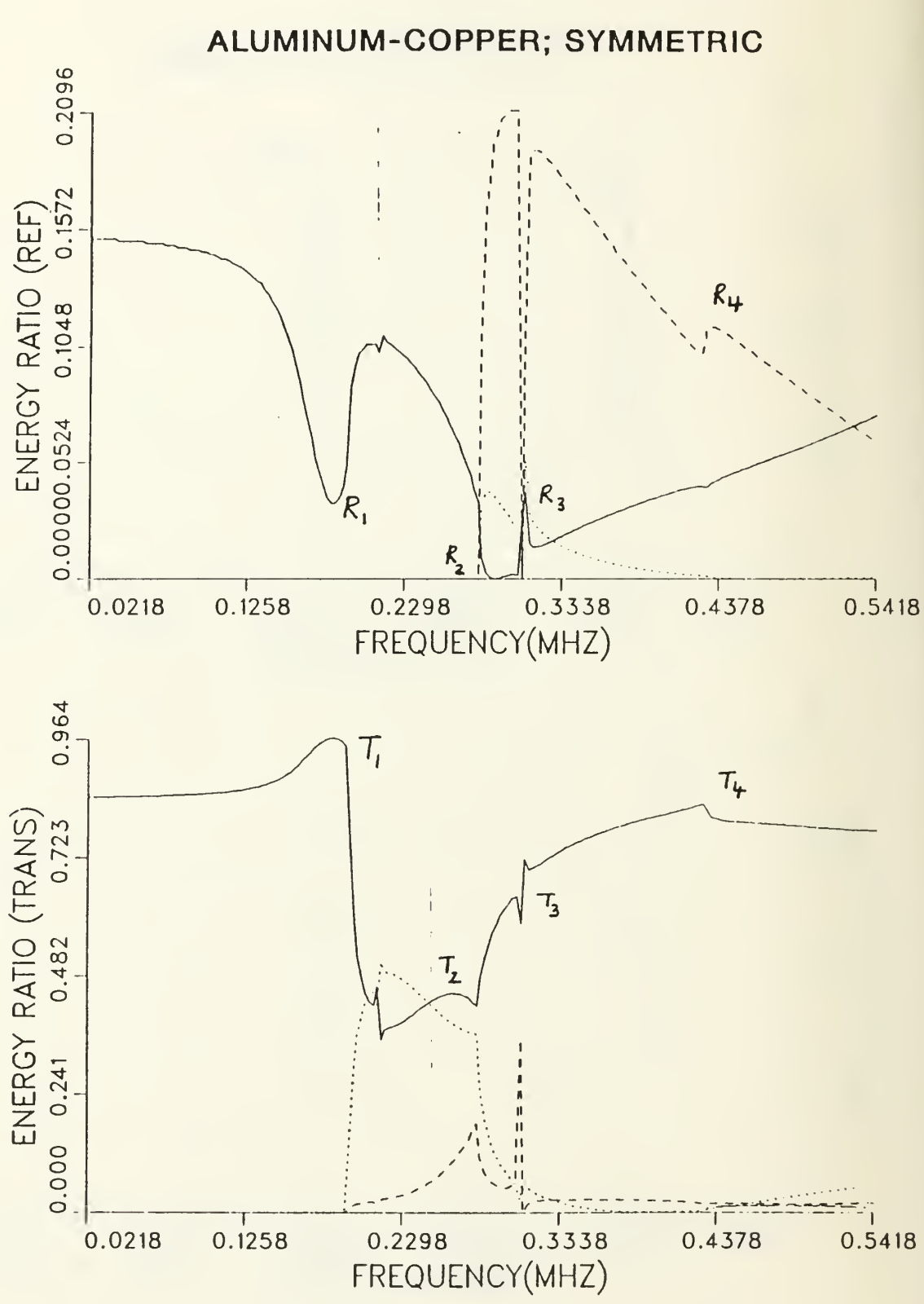
ALUMINUM-COPPER; SYMMETRIC
ENERGY RATIO (REF)
0.0000 0.0524 0.1048 0.1572 0.2096
R1
R2
R3
R4
0.0218 0.1258 0.2298 0.3338 0.4378 0.5418
FREQUENCY(MHZ)
ENERGY RATIO (TRANS)
0.000 0.241 0.482 0.723 0.964
T1
T2
T3
T4
0.0218 0.1258 0.2298 0.3338 0.4378 0.5418
FREQUENCY(MHZ)
Mode 1
Mode 2
Mode 3
Mode 4

Fig. 4

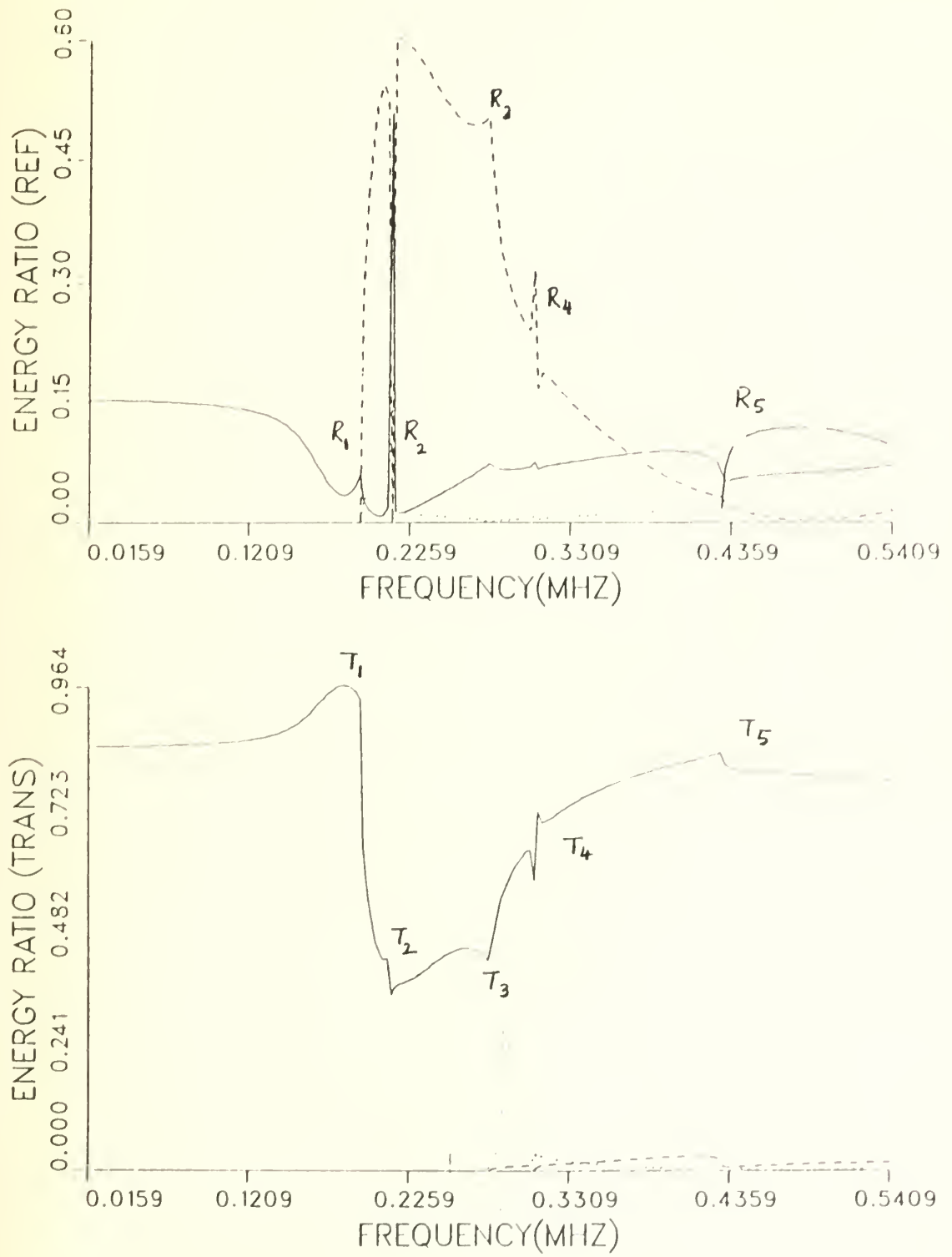
COPPER-ALUMINUM; SYMMETRIC
ENERGY RATIO (REF)
0.00
0.15
0.30
0.45
0.60
R1
R2
R3
R4
R5
0.0159
0.1209
0.2259
0.3309
0.4359
0.5409
FREQUENCY(MHZ)
ENERGY RATIO (TRANS)
0.000
0.241
0.482
0.723
0.964
T1
T2
T3
T4
T5
0.0159
0.1209
0.2259
0.3309
0.4359
0.5409
FREQUENCY(MHZ)
Mode 1
Mode 2
Mode 3
Mode 4

Fig. 5

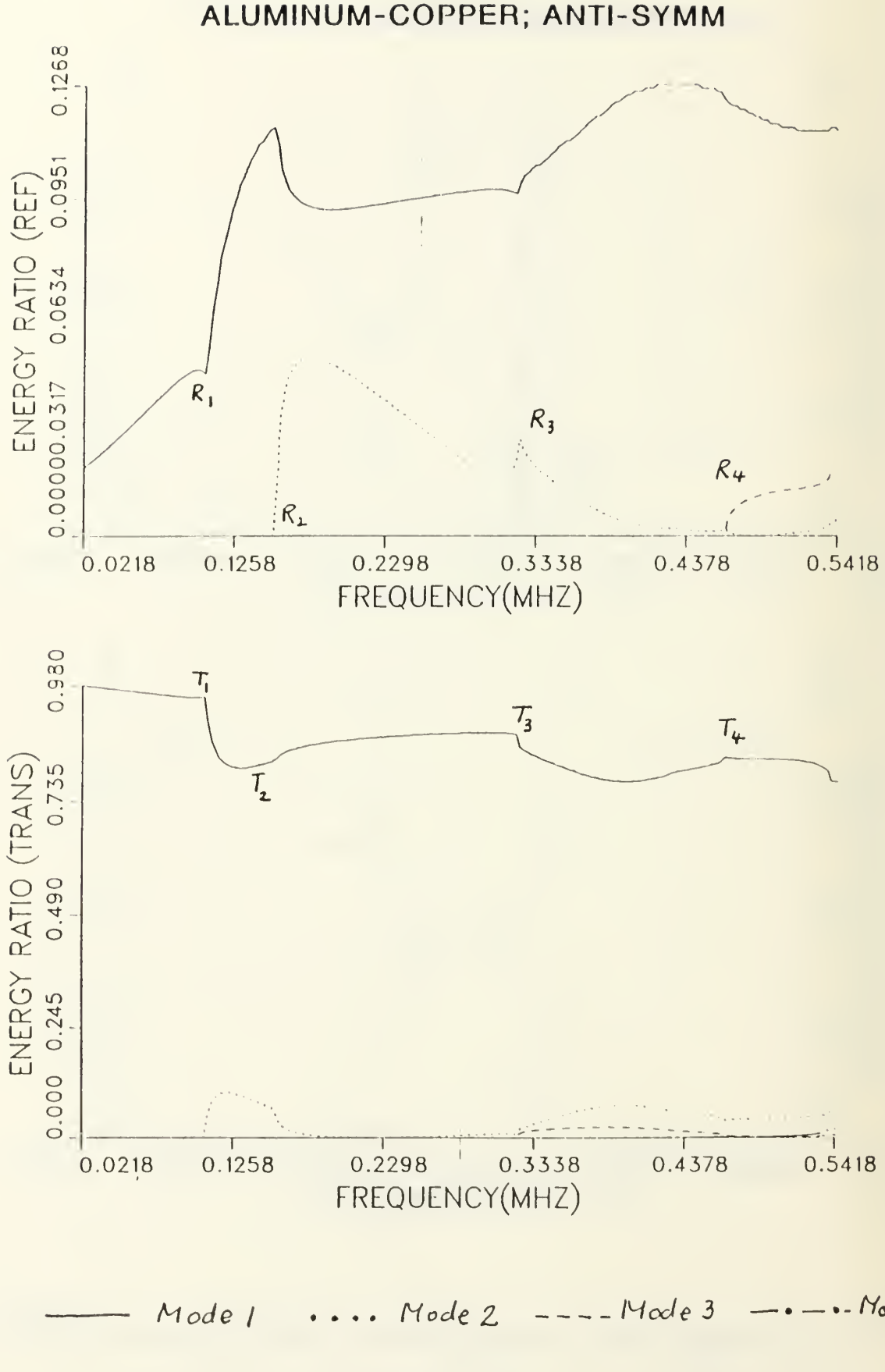
ALUMINUM-COPPER; ANTI-SYMM
ENERGY RATIO (REF)
0.00000.0317 0.0634 0.0951 0.1268
R1
R2
R3
R4
0.0218 0.1258 0.2298 0.3338 0.4378 0.5418
FREQUENCY(MHZ)
ENERGY RATIO (TRANS)
0.000 0.245 0.490 0.735 0.980
T1
T2
T3
T4
0.0218 0.1258 0.2298 0.3338 0.4378 0.5418
FREQUENCY(MHZ)
Mode 1
Mode 2
Mode 3
Mode 4

Fig. 6

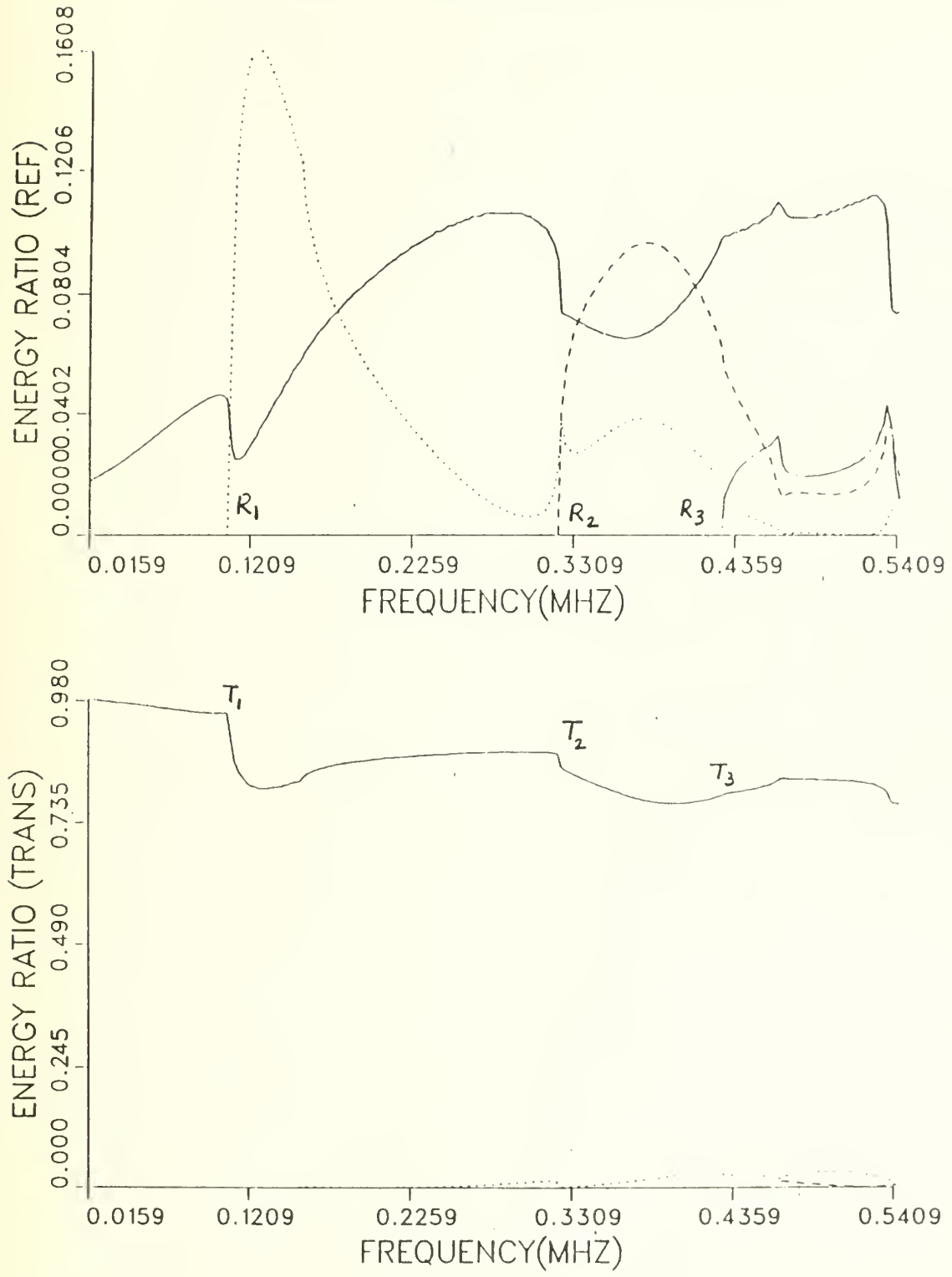
COPPER-ALUMINUM; ANTI-SYMM
ENERGY RATIO (REF)
0.00000.0402 0.0804 0.1206 0.1608
R1
R2
R3
0.0159 0.1209 0.2259 0.3309 0.4359 0.5409
FREQUENCY(MHZ)
ENERGY RATIO (TRANS)
0.000 0.245 0.490 0.735 0.980
T1
T2
T3
0.0159 0.1209 0.2259 0.3309 0.4359 0.5409
FREQUENCY(MHZ)
Mode1 Mode 2 Mode 3 Mode4

Fig. 7

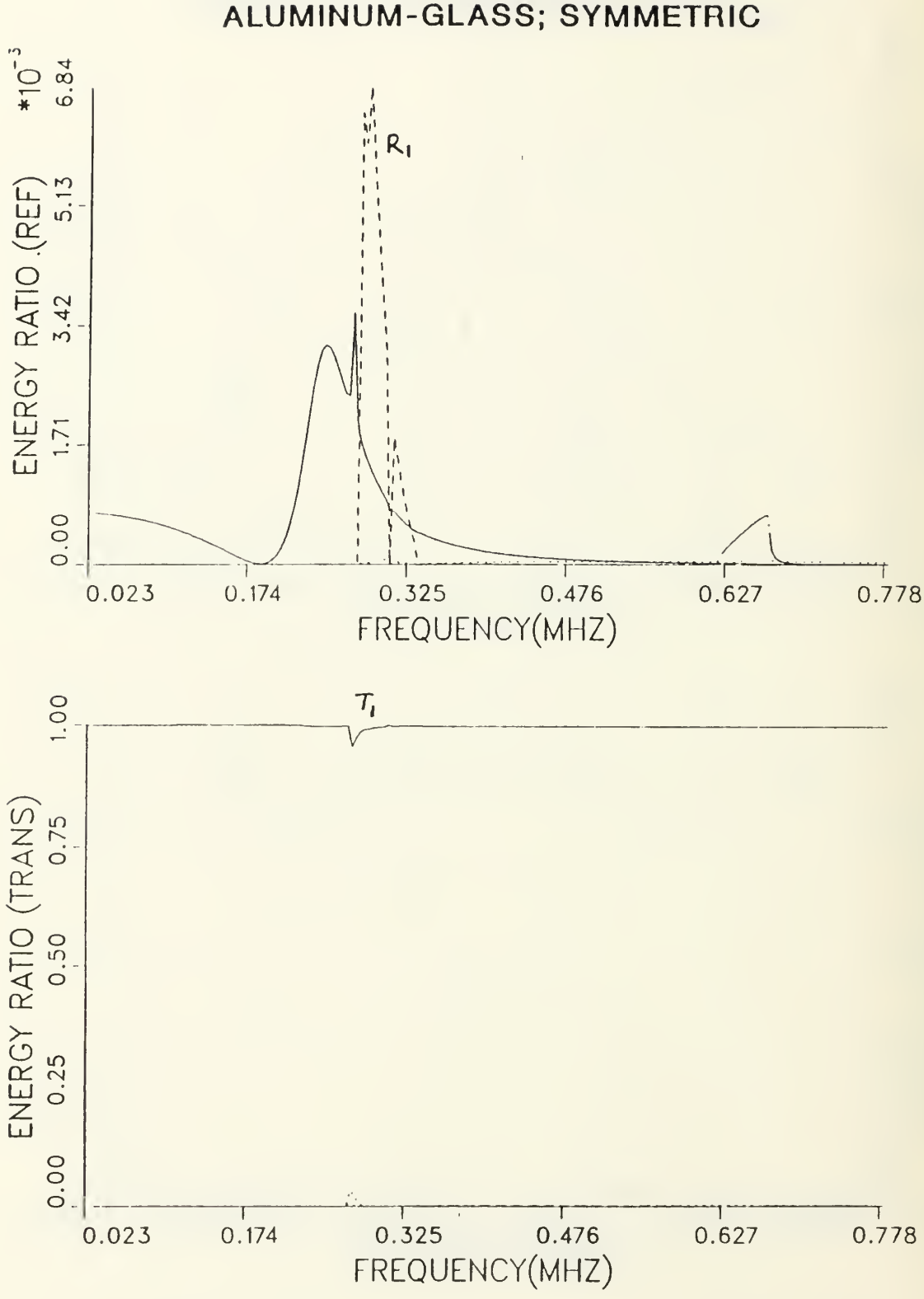

—— Mode 1 ····· Mode 2 ---- Mode 3 —·—·— Mode 4

Fig. 8

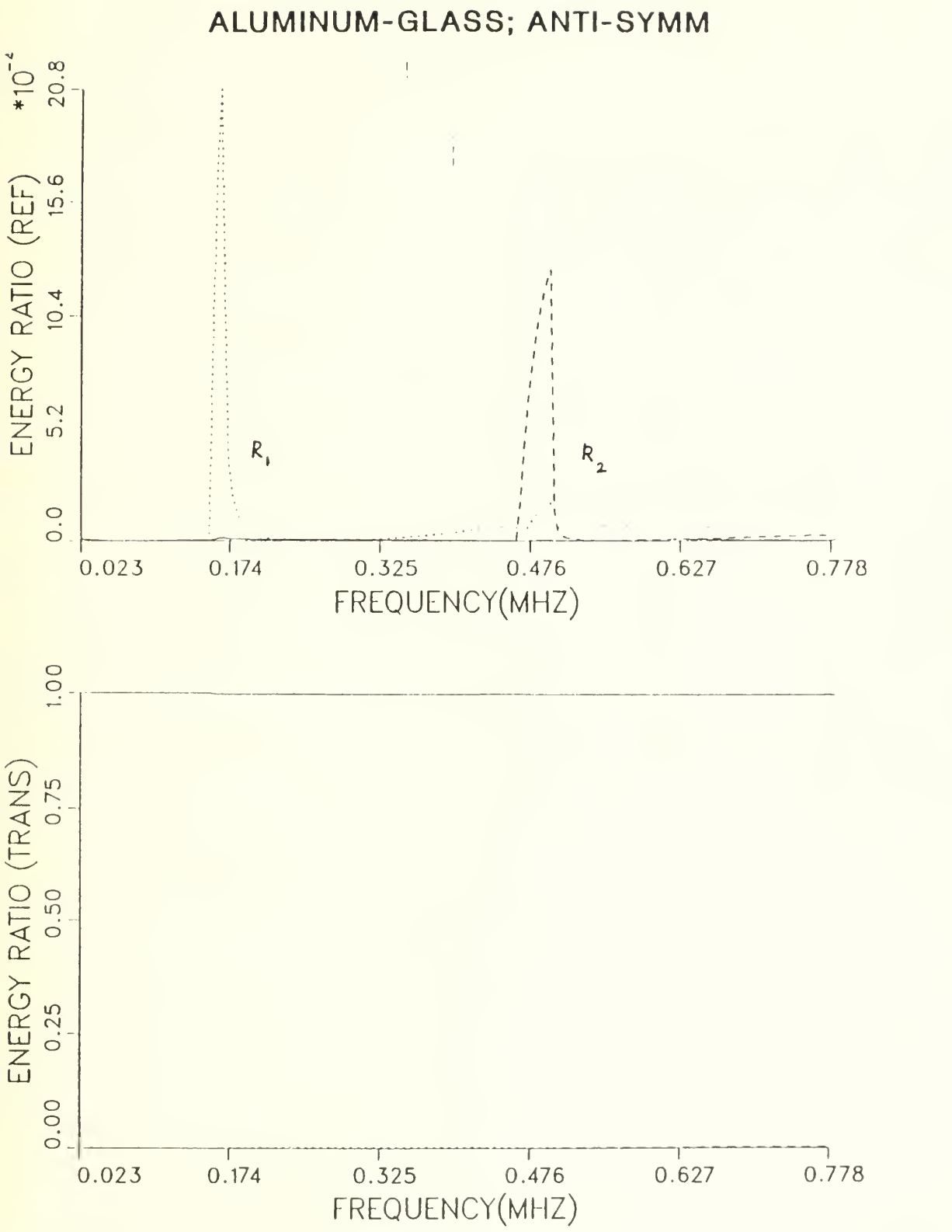
ALUMINUM-GLASS; ANTI-SYMM
ENERGY RATIO (REF)
*10⁻⁴
0.0
5.2
10.4
15.6
20.8
R1
R2
0.023
0.174
0.325
0.476
0.627
0.778
FREQUENCY(MHZ)
ENERGY RATIO (TRANS)
0.00
0.25
0.50
0.75
1.00
0.023
0.174
0.325
0.476
0.627
0.778
FREQUENCY(MHZ)
Mode 1
Mode 2
Mode 3
Mode 4

Fig. 9

INITIAL DISTRIBUTION LIST

DIRECTOR (2)
DEFENSE TECH. INFORMATION
CENTER, CAMERON STATION
ALEXANDRIA, VA 22314

CENTER FOR NAVAL ANALYSES
4401 FORD AVENUE
ALEXANDRIA, VA 22302-0268

LIBRARY (2)
CODE 0142
NAVAL POSTGRADUATE SCHOOL
MONTEREY, CA 93943

DIRECTOR OF RESEARCH ADMINISTRATION
CODE 012
NAVAL POSTGRADUATE SCHOOL
MONTEREY, CA 93943

DEPARTMENT OF MATEMATICS
CODE 53
NAVAL POSTGRADUATE SCHOOL
MONTEREY, CA 93943

ASST. PROFESSOR CLYDE SCANDRETT (20)
CODE 53Sd
DEPARTMENT OF MATHEMATICS
NAVAL POSTGRADUATE SCHOOL
MONTEREY, CA 93943

U.S. DEPARTMENT OF ENERGY
OFFICE OF ENERGY RESEARCH
WASHINGTON, DC 20545

PROF. STEVE BAKER
CODE 61Ba
DEPARTMENT OF PHYSICS
NAVAL POSTGRADUATE SCHOOL
MONTEREY, CA 93943

PROF. MEDWIN HERMANN
CODE 61 Me
DEPARTMENT OF PHYSICS
NAVAL POSTGRADUATE SCHOOL
MONTEREY, CA 93943

DUDLEY KNOX LIBRARY
3 2768 00335465 5